

Dimension transcendence and anomalous charge transport in magnets with moving multiple- Q spin textures

Ying Su,^{1,*} Satoru Hayami,² and Shi-Zeng Lin^{1,†}

¹Theoretical Division, T-4 and CNLS, Los Alamos National Laboratory, Los Alamos, New Mexico 87545, USA

²Department of Physics, Hokkaido University, Sapporo 060-0810, Japan

(Dated: November 17, 2021)

Multiple- Q spin textures, such as magnetic bubble and skyrmion lattices, have been observed in a large family of magnets. These spin textures can be driven into motion by external stimuli. The motion of spin textures affects the electronic states. Here we show that to describe correctly the electronic dynamics, the momentum space needs to be transcended to higher dimensions by including the ancillary dimensions associated with phason modes of the translational motion of the spin textures. The electronic states have non-trivial topology characterized by the first and second Chern numbers in the high dimensional hybrid momentum space. This gives rise to an anomalous electric charge transport due to the motion of spin textures. By deforming the spin textures, a nonlinear response associated with the second Chern number can be induced and results in the piezoelectricity. The charge transport is derived from the semi-classical equation of motion of electrons that depends on the Berry curvature in the hybrid momentum space. Our results suggest that the motion of multiple- Q spin textures has significant effects on the electronic dynamics and provides a new platform to explore high dimensional topological physics.

I. INTRODUCTION

Spatially localized spin textures with nontrivial topology, such as magnetic bubble and skyrmion, has been observed in several families of material systems including both metals and insulators, and heterostructures [1–4]. These spin textures form a lattice, which gives rise to several Bragg peaks associated with the lattice symmetry in the spin structure factor [1]. For this reason, these crystallized spin textures are also named as multiple- Q spin textures. The spin textures respond to various external stimuli, including electric current [5–7], electric field [8, 9], magnetic field [10, 11], thermal gradient [12–14], and strain [15–17], which renders them as very promising entities for applications [18–20].

The *static* spin texture has significant effects on electronic wave functions and affects the dynamics of conduction electrons [21, 22]. For instance, when electrons interact with a *static* skyrmion, they experience an effective magnetic field produced by the noncoplanar spin texture. As a consequence, there is a topological Hall effect, which has been observed experimentally [23–25]. The noncoplanar spin texture can open an energy gap in the electronic spectrum and stabilize a Chern insulator [22, 26–28]. The spin texture can be driven into motion by magnetic or electric field gradients [9–11], thermal gradients [12–14], and spin-polarized currents [29–31]. How the *motion* of spin textures affects the electronic dynamics is an important question. In ferromagnetic metals, the interaction between conduction electrons and moving spin textures can generate an emergent electric field that results in a spin motive force affecting the electronic dynamics [7, 32–34]. Nevertheless, how it works for a gapped system is not well understood.

In this paper, we reveal that the description of the dynam-

ics of conduction electrons coupled to the moving multiple- Q spin textures requires a transcendent high dimensional momentum space. The high dimensional momentum space is spanned by the physical dimensions and ancillary dimensions associated with phason modes of the translational motion of spin textures. The electronic states can have nontrivial topology characterized by the first and second Chern numbers in the hybrid momentum space when the energy spectrum is gapped. Due to the nontrivial topology, there is an anomalous charge transport in magnets with *moving* multiple- Q spin textures. To explain the anomalous charge transport, we develop a general semi-classical theory to study the response of electronic states to the motion and deformation of spin textures. Our results demonstrate that the motion of multiple- Q spin textures has profound consequences on the electronic wave functions and dynamics.

II. MODEL AND DIMENSION TRANSCENDENCE

The interaction between conduction electrons and spin textures can be described by the Hamiltonian

$$\mathcal{H} = -t \sum_{\langle i,j \rangle} c_i^\dagger c_j - J \sum_i c_i^\dagger \mathbf{S}_i \cdot \boldsymbol{\sigma} c_i - B \sum_i c_i^\dagger \sigma_z c_i, \quad (1)$$

where $c_i = (c_{i,\uparrow}, c_{i,\downarrow})^\top$ is the annihilation operator of conduction electrons with spin \uparrow and \downarrow at the i th site, $\langle i, j \rangle$ denotes two nearest-neighbor sites on a 2D square lattice, $\boldsymbol{\sigma}$ represents the vector of Pauli matrices, and \mathbf{S}_i encodes the spin texture. Here we assume that the spin texture \mathbf{S}_i is stabilized by other stronger interactions and is not affected by the conduction electrons. The spin configuration of the multiple- Q spin textures can be generally described by

$$\mathbf{S}_i = \sum_{\nu} G_{\nu}^{\mu}(\mathbf{Q}_{\nu} \cdot \mathbf{r}_i + \phi_{\nu}) \hat{\mathbf{e}}_{\mu}, \quad (2)$$

where $G_{\nu}^{\mu}(\phi_{\nu}) = G_{\nu}^{\mu}(\phi_{\nu} + 2\pi)$ and the Einstein summation convention is employed hereafter. The translational motion of the

* yingsu@lanl.gov

† szl@lanl.gov

spin texture, $\mathbf{r}_i \rightarrow \mathbf{r}_i + \mathbf{v}\tau$, is depicted by the phase $\phi_\nu = \mathbf{Q}_\nu \cdot \mathbf{v}\tau$, where \mathbf{v} is velocity and τ is time.

The coupling of conduction electrons to multiple- Q spin textures yields a magnetic superlattice. We denote the crystal momentum of the magnetic superlattice as \mathbf{k} . The Hamiltonian in the momentum space is also a periodic function of ϕ_ν besides \mathbf{k} , i.e. $H(\mathbf{k}, \boldsymbol{\phi})$ with $\boldsymbol{\phi} = (\phi_1, \phi_2, \dots)$. Therefore, when the spin texture is moving, the electronic dynamics is depicted in the effective momentum space spanned by $\tilde{\mathbf{k}} = \mathbf{k} \oplus \boldsymbol{\phi} = (k_x, k_y, \phi_1, \phi_2, \dots)$, a hybridization of crystal momenta and phason modes of the translational motion of spin textures. The motion of the spin textures is slow compared to electronic dynamics. For instance, for a spin texture with period 1 nm moving at a velocity 1 m/s, ϕ_ν changes at a rate of 1 GHz. As a good approximation, the electronic spectrum $E_n(\tilde{\mathbf{k}})$ and the corresponding eigenstate $|\psi_{n\tilde{\mathbf{k}}}\rangle$ evolve adiabatically with ϕ_ν .

III. NONLINEAR RESPONSE

The semi-classical equation of motion for an electronic wave packet with the dispersion $E_n(\tilde{\mathbf{k}})$ and center of mass \mathbf{r}_n follows

$$\dot{\mathbf{r}}_n^\mu = \frac{\partial E_n(\tilde{\mathbf{k}})}{\hbar \partial \tilde{k}_\mu} - \dot{\tilde{k}}_\nu \Omega_n^{\mu\nu}(\tilde{\mathbf{k}}), \quad (3)$$

where $\Omega_n^{\mu\nu} = i\partial_{\tilde{k}_\mu} \langle u_{n\tilde{\mathbf{k}}} | \partial_{\tilde{k}_\nu} u_{n\tilde{\mathbf{k}}} \rangle - i\partial_{\tilde{k}_\nu} \langle u_{n\tilde{\mathbf{k}}} | \partial_{\tilde{k}_\mu} u_{n\tilde{\mathbf{k}}} \rangle$ is the Berry curvature and $|u_{n\tilde{\mathbf{k}}}\rangle$ is the periodic part of the Bloch state $|\psi_{n\tilde{\mathbf{k}}}\rangle$. Eq. (3) is meaningful only when $\mu = x$ or y since the center of mass \mathbf{r}_n is confined in the real space. Here the first term is the group velocity and the last term is the anomalous velocity due to nonzero Berry curvatures [35]. In the absence of external electromagnetic fields, $\dot{\tilde{k}}_\nu = \dot{k}_\nu = 0$ for $\nu = \{x, y\}$. However, the translational motion of spin textures described by $\phi_\nu = \omega_\nu \tau$ ensures a nonzero $\dot{\tilde{k}}_\nu = \dot{\phi}_\nu = \omega_\nu$ for $\nu = \{1, 2, \dots\}$. In addition to the conventional anomalous velocity $-\dot{k}_\nu \Omega_n^{\mu\nu}(\tilde{\mathbf{k}})$ [35], there is a new contribution $-\dot{\phi}_\nu \Omega_n^{\mu\nu}(\tilde{\mathbf{k}})$ that can be obtained in the semi-classical theory (see Appendix A-C). The Berry curvature in the new contribution is defined in the hybrid momentum space consist of the crystal momentum k_μ and phason mode ϕ_ν . The semi-classical equation of motion is derived in the leading order. The higher order corrections do not change the form of equation of motion but modify the dispersion relation and Berry curvature due to interband coupling (see Appendix B). Since the higher order corrections do not change our finally results (proved in Appendix D), the modifications of dispersion relation and Berry curvature are not considered here. The corresponding current density due to the translational motion of spin textures is

$$\mathbf{j}_0^\mu = e \sum_n \int \frac{d^2k}{4\pi^2} f(E_n - E_F) \left(\frac{\partial E_n}{\hbar \partial k_\mu} - \omega_\nu \Omega_n^{\mu\nu} \right), \quad (4)$$

where $f(E_n - E_F)$ is the Fermi distribution function and E_F is the Fermi energy. When the energy spectrum is gapped in the hybrid momentum space and the Fermi energy E_F is in the

gap, the first term in Eq. (4) vanishes. The transported charge over one period $\Delta\tau = 2\pi/|\omega_\nu|$ at zero temperature is

$$q_0^\mu = -\frac{eN^\mu}{|\omega_\nu|} \sum_{E_n \leq E_F} \int_0^{2\pi} d\phi_\nu \int \frac{d^2k}{4\pi^2} \omega_\nu \Omega_n^{\mu\nu} = \frac{eN^\mu \omega_\nu C_1^{\mu\nu}}{|\omega_\nu|}, \quad (5)$$

$$C_1^{\mu\nu} = -\frac{1}{2\pi} \sum_{E_n \leq E_F} \int dk_\mu d\phi_\nu \Omega_n^{\mu\nu}, \quad (6)$$

where $C_1^{\mu\nu}$ is the first Chern number defined on the $\tilde{k}_\mu \tilde{k}_\nu$ plane and is independent of the other momenta if the energy gap retains open in the entire hybrid momentum space, and N^μ is the number of unit cells in the cross section perpendicular to the μ direction. Therefore the translational motion of the spin textures can result in quantized charge transport in magnetic insulators with $C_1^{\mu\nu} \neq 0$, which is the topological pumping.

The response function Eq. (4) becomes nonlinear when the dynamics of ϕ_ν couples with $\dot{\mathbf{r}}_n$. This can be achieved by deforming the spin texture, $\mathbf{Q}_\nu \rightarrow \mathbf{Q}_\nu + \mathbf{Q}'_\nu$. Therefore, $\phi_\nu = \omega_\nu \tau + \mathbf{Q}'_\nu \cdot \mathbf{r}_n$, and its dynamics follows

$$\dot{\tilde{k}}_\nu = \dot{\phi}_\nu = \omega_\nu + \mathbf{Q}'_{\nu\mu} \dot{\mathbf{r}}_n^\mu, \quad (7)$$

that depends on the velocity of wave packet (see Appendix A). Substituting Eq. (7) into Eq. (3) and retaining the terms up to the second order in ω_ν and $\mathbf{Q}'_{\nu\mu}$, we obtain

$$\dot{\mathbf{r}}_n^\mu = \frac{\partial E_n}{\hbar \partial k_\mu} - \omega_\nu \Omega_n^{\mu\nu} - \left(\frac{\partial E_n}{\hbar \partial k_\gamma} - \omega_\delta \Omega_n^{\gamma\delta} - \frac{\partial E_n}{\hbar \partial k_\eta} \mathbf{Q}'_{\delta\eta} \Omega_n^{\gamma\delta} \right) \mathbf{Q}'_{\nu\gamma} \Omega_n^{\mu\nu}, \quad (8)$$

where the first two terms correspond to the linear response in Eq. (4). The last term in Eq. (8) originated from the deformation of spin textures induces a nonlinear response

$$\mathbf{j}^\mu = \mathbf{j}_0^\mu + e \sum_n \int \frac{d^2k}{8\pi^2} f(E_n - E_F) F_n^{\mu\nu\gamma\delta} \omega_\nu \mathbf{Q}'_{\gamma\delta}, \quad (9)$$

where $F_n^{\mu\nu\gamma\delta} = \Omega_n^{\mu\nu} \Omega_n^{\gamma\delta} + \Omega_n^{\mu\gamma} \Omega_n^{\delta\nu} + \Omega_n^{\mu\delta} \Omega_n^{\nu\gamma}$ (see Appendix D). In this case, the transported charge over $\Delta\tau$ at zero temperature is

$$\begin{aligned} q^\mu &= q_0^\mu + \frac{eL^\mu}{|\omega_\nu|} \int_0^{2\pi} d\phi_\nu \sum_{E_n \leq E_F} \int \frac{d^2k}{8\pi^2} F_n^{\mu\nu\gamma\delta} \omega_\nu \mathbf{Q}'_{\gamma\delta} \\ &\approx q_0^\mu + \frac{eL^\mu C_2^{\mu\nu\gamma\delta} \omega_\nu \mathbf{Q}'_{\gamma\delta}}{4\pi|\omega_\nu|} \end{aligned} \quad (10)$$

where L^μ is the size of the cross section perpendicular to the μ direction and

$$C_2^{\mu\nu\gamma\delta} = \frac{1}{4\pi^2} \sum_{E_n \leq E_F} \int dk_\mu d\phi_\nu dk_\gamma d\phi_\delta F_n^{\mu\nu\gamma\delta}, \quad (11)$$

is the second Chern number [36] defined on the $\tilde{k}_\mu \tilde{k}_\nu \tilde{k}_\gamma \tilde{k}_\delta$ hypersurface of the hybrid momentum space. Here we make the approximation that $F_n^{\mu\nu\gamma\delta} \approx \int d\phi_\delta F_n^{\mu\nu\gamma\delta} / 2\pi$. The approximation is valid when the Berry curvatures are weakly dispersive

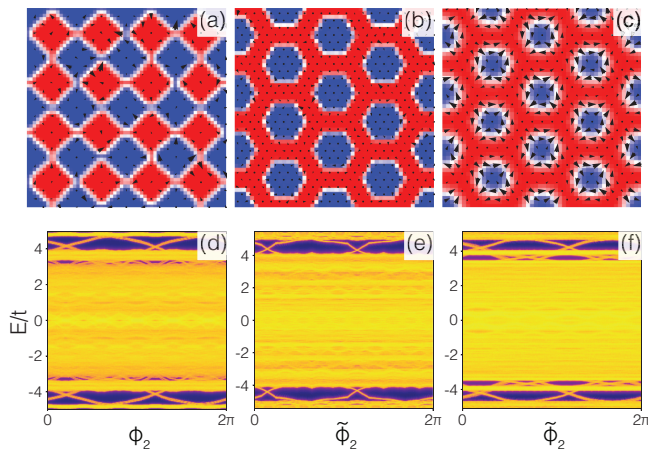


FIG. 1. Spin textures obtained from the Monte Carlo simulation. (a) The double- Q collinear magnetic bubble lattice. (b) The triple- Q collinear magnetic bubble lattice. (c) The triple- Q skyrmion lattice. Here the arrows represent the in-plane components and the background color (with red for positive and blue for negative) stands for the z component of local spins. (d-f) Electronic spectral functions as a function of ϕ_2 ($\tilde{\phi}_2$) for conduction electrons coupled to the three spin textures (a)-(c), respectively. Here the purple (yellow) denotes low (high) density of states.

as a function of ϕ_δ . This is true when the spin texture is incommensurate with the lattice or the period of spin texture is much larger than the lattice constant. In our definition, both $C_1^{\mu\nu}$ and $C_2^{\mu\nu\gamma\delta}$ are antisymmetric under the permutation of the indices because $\Omega_n^{\mu\nu} = -\Omega_n^{\nu\mu}$. Equation (10) demonstrates that, in addition to the contribution from the first Chern number, the charge transport has the contribution from the second Chern number when the spin texture is deformed.

To substantiate the anomalous charge transport due to the translational motion of the spin textures from the semiclassical analysis above, we study the charge transport in magnets with several typical multiple- Q spin textures obtained from the Monte Carlo simulation (see Appendix E). Here we consider three kinds of spin textures: double- Q and triple- Q collinear magnetic bubble lattices where spins are nearly parallel or antiparallel due to the strong easy axis anisotropy, and triple- Q skyrmion lattice as shown in Figs. 1(a)-1(c), respectively. For conduction electrons hopping on a square lattice (whose lattice constant is set to unity), the \mathbf{Q}_ν vectors for the double- Q magnetic bubble lattice are $\mathbf{Q}_1 = (2\pi/5, 0)$ and $\mathbf{Q}_2 = (0, 2\pi/5)$, while for the triple- Q magnetic bubble and skyrmion lattices are $\mathbf{Q}_1 = (-2\pi/5, 2\sqrt{3}\pi/5)$, $\mathbf{Q}_2 = (-2\pi/5, -2\sqrt{3}\pi/5)$, and $\mathbf{Q}_3 = (4\pi/5, 0)$. For the triple- Q states, because $\sum_{\nu=1}^3 \phi_\nu = 0$ for a translational motion, only two of ϕ_ν are independent of each other.

IV. TOPOLOGICAL PROPERTY

To identify the topology of electronic states in magnets with the multiple- Q spin textures, we first study their electronic

spectra in the hybrid momentum space. For the double- Q magnetic bubble lattice, the translational motion of the spin texture is parameterized by $\phi_\nu = \omega_\nu \tau$. The energy spectrum as a function of ϕ_2 (with $\phi_1 = 0$) is shown in Figs. 1(d) for the double- Q spin texture with $J = 1.5t$ and $B = 0$. Here we use the periodic boundary condition along the x direction and the open boundary condition along the y direction. Apparently, there are topological edge states in the bulk energy gaps indicating the system is topologically nontrivial. For the triple- Q spin textures, to make them commensurate with the lattice, we compress the lattice constant along the y direction to $1/\sqrt{3}$. In this case, because $\sum_{\nu=1}^3 \phi_\nu = 0$, we define $\tilde{\phi}_1 = -(\phi_1 + \phi_2)/2 = \phi_3/2$ and $\tilde{\phi}_2 = (\phi_1 - \phi_2)/2$ that are independent. The change of $\tilde{\phi}_1$ and $\tilde{\phi}_2$ corresponds to the shift of triple- Q spin textures along the x and y directions, respectively. Thus we can parameterize the translational motion of the triple- Q spin textures by $\tilde{\phi}_\nu = \omega_\nu \tau$. The energy spectra as a function of $\tilde{\phi}_2$ (with $\tilde{\phi}_1 = 0$) for the triple- Q magnetic bubble and skyrmion lattices with $J = 1.5t$ and $B = -1.2t$ are displayed in Figs. 1(e) and 1(f), respectively. The topological edge states and bulk energy gaps persist for the triple- Q spin textures.

To characterize the nontrivial band topology, we calculate the Chern numbers of the system with an efficient algorithm by using the $U(1)$ link variable [37, 38]. For commensurate spin textures, the system has translational symmetry and we can describe it in a high dimensional hybrid momentum space spanned by the generalized crystal momentum $\tilde{\mathbf{k}} = (k_x, k_y, \phi_1, \phi_2)$ for the double- Q spin texture and $\tilde{\mathbf{k}} = (k_x, k_y, \tilde{\phi}_1, \tilde{\phi}_2)$ for the triple- Q spin textures. Even if the spin texture is incommensurate with the lattice, k_x and k_y can still be introduced by using the twisted boundary condition [39]. Consequently, the Chern numbers in Eqs. (6) and (11) are well defined on the compact manifold. As an example, we consider the Fermi energy in the bottom bulk energy gaps in Figs. 1(d)-1(f). In the 4D hybrid momentum space, there are six first Chern numbers: $C_1^{x1} = C_1^{y2} = 2$ and $C_1^{xy} = C_1^{x2} = C_1^{y1} = C_1^{12} = 0$, and one second Chern number: $C_2^{x1y2} = -2$ for the double magnetic bubble lattice. For the triple- Q magnetic bubble and skyrmion lattices, they have the same Chern numbers: $C_1^{x1} = C_1^{y2} = 2$, $C_1^{xy} = C_1^{x2} = C_1^{y1} = C_1^{12} = 0$, and $C_2^{x1y2} = -4$. Interestingly, our results demonstrate an insulator that is trivial in the crystal momentum space, can be topologically nontrivial in the hybrid momentum space.

V. ANOMALOUS CHARGE TRANSPORT

The translational motion of spin textures can induce a quantized charge transport according to Eqs. (5) and (6). Here we consider the spin textures shifting along the y direction on a 40×40 lattice (containing 8×8 supercells) with $\omega_1 = 0$ and $\omega_2 = 2\pi t/100\hbar$, and we calculate the electric currents of the system by solving the time-dependent Schrödinger equation (see Appendix F). We focus on the Fermi energy in the bottom bulk energy gaps in Figs. 1(d)-1(f). For the double- Q

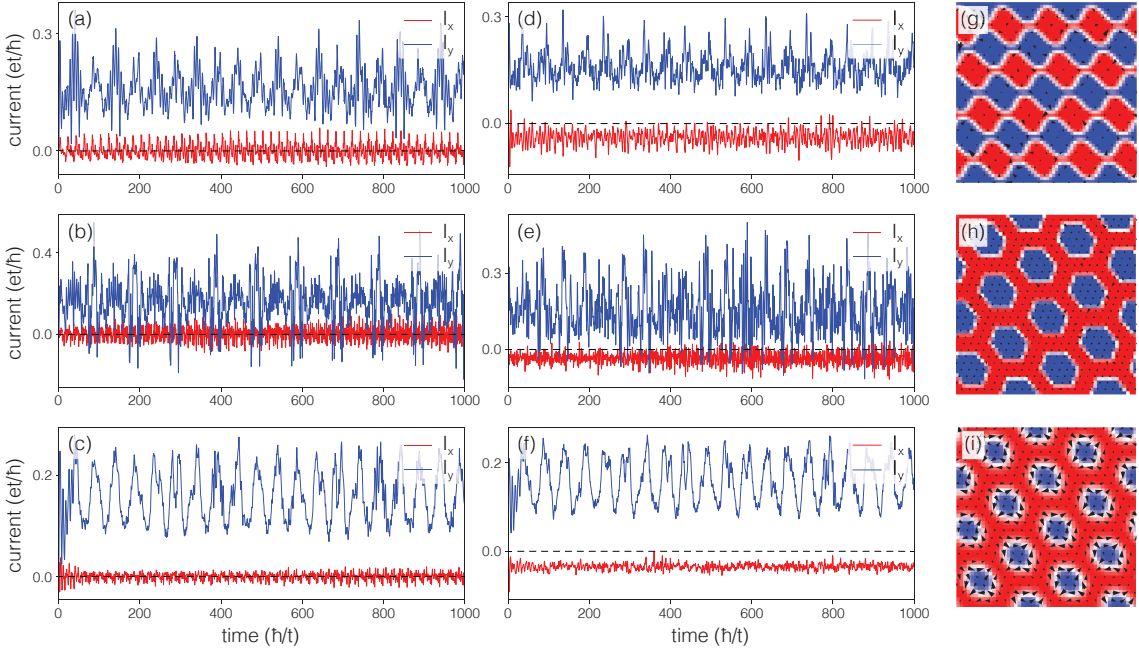


FIG. 2. Currents along the x and y directions induced by the translational motion of spin textures. (a) Currents for the double- Q magnetic bubble lattice in Fig. 1(a), (b) currents for the triple- Q magnetic bubble lattice in Fig. 1(b), and (c) currents for the triple- Q skyrmion lattice in Fig. 1(c). (d)-(f) Currents for the three spin textures under a shear deformation. (g)-(i) Sheared spin textures are obtained by applying a shear strain on the spin textures in Fig. 1(a)-(c).

magnetic bubble lattice, the currents along the x and y directions over ten periods are shown in Fig. 2(a). By integrating the currents over time, the average transported charges in one period are $q^x = 0.01e$ and $q^y = 15.95e$. According to Eq. (5), $q^x = eN^x\omega_2C^{x2}/|\omega_2| = 0$ and $q^y = eN^y\omega_2C^{y2}/|\omega_2| = 16e$. Apparently, the number obtained by simulation shows a good agreement with that obtained from the semi-classical equation. For the triple- Q magnetic bubble lattice, we have $q^x = 0.14e$ and $q^y = 16.04e$ from the currents in Fig. 2(b), while for the triple- Q skyrmion lattice, we have $q^x = 0.00e$ and $q^y = 15.96e$ from the currents in Fig. 2(c). The numerical results for the triple- Q spin textures are also consistent with $q^x = 0$ and $q^y = 16e$ obtained from Eq. (5).

The nonlinear response can be realized by deforming the spin texture as shown in Eqs. (7) and (9). For the double- Q magnetic bubble lattice, we deform the spin texture by setting $\phi_1 = \mathbf{Q}'_1 \cdot \mathbf{r}$ with $\mathbf{Q}'_1 = (0, 2\pi/20)$. This induces a shear strain $\gamma_{xy} = -Q'_{1y}/Q_{1x} = -0.25$ on the spin texture that results in $x \rightarrow x + \gamma_{xy}y$, as shown in Fig. 2(g). The currents due to the translational motion and shear strain of the spin texture are displayed in Fig. 2(d). In this case, the transported charges in one period are $q^x = -3.92e$ and $q^y = 15.89e$ from the currents in Fig. 2(d). Meanwhile, according to the Eq. (10), we have $q^x = eL^xC_2^{x21y}\omega_2Q'_{1y}/2\pi|\omega_2| = -4e$ where $C_2^{x21y} = C_2^{x1y2} = -2$, and $q^y = 16e$ as before. The results from numerical simulation and semi-classical analysis are consistent with each other. Therefore, we demonstrate that, besides the longitudinal charge transport due to the linear response, there is a transverse charge transport caused by the nonlin-

ear response of the deformed spin texture. Moreover, one can probe the Chern numbers experimentally from the quantized charge transport. For the triple- Q spin textures, the shear strain can also be induced by taking $\tilde{\phi}_1 = \mathbf{Q}'_1 \cdot \mathbf{r}$, where we set $\mathbf{Q}'_1 = (0, 2\sqrt{3}\pi/40)$ and $\gamma_{xy} = Q'_{1y}/Q_{1x} = -0.125\sqrt{3}$ in Figs. 2(h) and 2(i). The currents of the triple- Q magnetic bubble lattice are shown in Fig. 2(e) and the transported charges in one periodic are $q^x = -3.43e$ and $q^y = 15.60e$. The currents of the triple- Q skyrmion lattice are shown in Fig. 2(f) and the transported charges are $q^x = -3.48e$ and $q^y = 15.92e$. Equation (10) yields $q^x = -4e$ and $q^y = 16e$ for the triple- Q spin textures. In this case, the numerical results are less quantized. One possible reason is due to the fact that the spin textures from Monte Carlo simulation are not exactly periodic. As a comparison, we also calculate the current for the double- Q and triple- Q spin texture ansatz described by the linear superposition of cosine functions, and the transported charge for the ansatz are perfectly quantized (see Appendix G).

When the deformed spin texture is commensurate with the lattice, one may wonder whether the anomalous charge transport can be fully characterized by the first Chern numbers of the deformed system. To answer this question, we take the deformed double- Q magnetic bubble lattice studied above as an example. Under the deformation induced by $\mathbf{Q}'_1 = (0, 2\pi/20)$, the new unit cell is enlarged to contain 5×20 lattice sites (fourth larger than the undeformed unit cell that is 5×5). Therefore on the 40×40 lattice, $N_x = 2$ and $N_y = 8$. Because the lattice constant along the y direction is increased by 4 times, the period of motion of the spin texture is also in-

creased by 4 times (since ω_2 is fixed). By performing exactly the same calculation, we find the relevant first Chern numbers of the deformed system become $C_1^{x2} = -8$ and $C_1^{y2} = 8$. Plugging these into Eq. (5), we get $q^x = -16e$ and $q^y = 64e$ in one period of motion. To compare with the previous results, we need to divide the new q^x and q^y by 4 to count the transported charges in the same period of time as the undeformed case. Thus, the two independent approaches yield the same result. As shown in this example, even a small deformation of spin textures can increase the size of unit cell significantly. With the periodic modulation extended to a larger length scale, there are more energy bands due to the band folding, accompanying complicated band gap closing and opening in this process, where the topological phase transitions are possible. Therefore, without the nonlinear response function associated with the second Chern number, one needs to calculate different first Chern numbers for different deformation to understand the charge transport. This calculation turns out to be impractical for small deformation that results in huge unit cells. In this sense, the nonlinear response theory can make life much easier since one only needs to know the first and second Chern numbers of the undeformed system and these Chern numbers are usually relatively easy to calculate.

VI. LINEAR PIEZOELECTRICITY.

As we have shown above, the deformation of spin textures is essential to generate the nonlinear response. The deformation of magnetic skyrmion lattices has been realized in a strained crystal [17] or by applying an electric field [40]. Very recently, the deformation of the moving magnetic skyrmion lattice under electric current flow has also been observed [41]. According to Eq. (9), the current depends linearly on the deformed \mathcal{Q}'_v vector, i.e. $j^\mu \propto \mathcal{Q}'_{v\delta}$. For instance, when the spin texture is deformed by an effective shear strain $\gamma_{xy} \propto \mathcal{Q}'_{1y}$ in our numerical simulation above, the linear piezoelectric current is $j^x \propto \gamma_{xy}$. To verify the linear piezoelectricity, we calculate q^x as a function of γ_{xy} and we expect $q^x \propto \gamma_{xy}$. The numerical results are displayed in Fig. 3. For the finite system size (40×40 lattice sites) considered in our numerical calculations, the shear strain are limited to a few discrete values in order to retain the periodic boundary condition. For much larger systems, the shear strain can be tuned continuously. We show q^x as a function of γ_{xy} for the double- Q magnetic bubble lattice in Fig. 3(a), and for the triple- Q magnetic bubble and skyrmion lattices in Fig. 3(b). Here the symbols are from the numerical calculation and the black lines are from the Eq. (10). Apparently, the q^x for the double- Q spin texture collapses on the black line and shows a good linear dependence on γ_{xy} . The q^x for the triple- Q spin textures are also linear in γ_{xy} but deviate from the black line due to poor quantization of charge transport as reasoned above. Therefore, the linear piezoelectricity is verified numerically and works for moderate strains that preserve the intrinsic topology. Our results suggest a new mechanism of piezoelectricity as a consequence of the nontrivial topology.

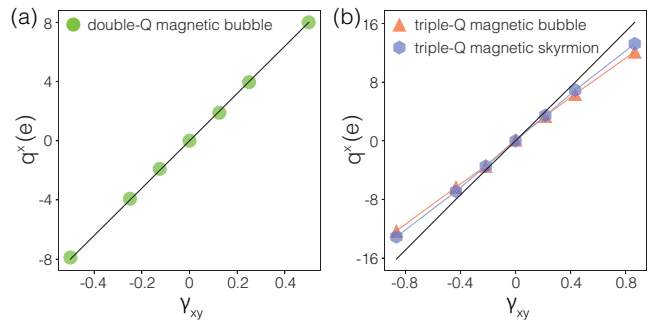


FIG. 3. Linear piezoelectricity induced by the deformation of spin textures. (a) q^x as a function of the deformation γ_{xy} for the double- Q magnetic bubble lattice, and (b) for the triple- Q magnetic bubble and skyrmion lattices. The black lines are from the response function Eq. (10).

VII. DISCUSSION

The nonlinear response due to the translational motion and deformation of the spin textures is associated with the second Chern number. The quantized charge transport requires the Fermi energy in the bulk energy gap. When this is not the case, Eq. (9) is still valid but the transported charge is not quantized. Therefore, the anomalous charge transport generated by the motion of spin textures occurs both in insulating and metallic magnets. In our system, the electronic dynamics is governed by the nontrivial topology of electronic structure in the hybrid momentum space spanned by the crystal momentum and phason mode of the spin texture. This is different from the emergent electrodynamics induced by the motion of non-collinear spin textures according to the generalized Faradays law [7, 32, 33] or magnetization dynamics as a reciprocal process of the spin transfer torque [34]. Evidently, the anomalous charge transport in the collinear spin textures and in magnetic insulators can not be captured by the emergent electrodynamics. Our predictions can be tested in B20 chiral magnets [1, 2], f -electron materials [42, 43] and magnetic heterostructures [44–46], where multiple- Q spin textures have been observed in experiments. The quantized charge transport can be possibly realized in a heterostructure with the multiple- Q spin texture formed in a magnetic insulator layer or at the interface through the proximity effect [47–49]. In materials, the multiple- Q spin textures are pinned by defects. To drive the spin texture into motion, a large driving force is needed in order to overcome the pinning energy. The pinning-depinning transition provides a clear way to distinguish the anomalous charge transport from other contributions.

In summary, we reveal that the motion of spin textures has significant effects on the dynamics of conduction electrons. The semi-classical equation of motion of the electronic wave packet is described in a high dimensional hybrid momentum space. The hybrid momentum space is constituted of the physical dimensions and ancillary dimensions associated with the phason modes of the translational motion of the spin textures. The electronic states can be topologically nontrivial when the

energy spectrum is gapped, and the nontrivial topology is characterized by the first and second Chern numbers in the hybrid momentum space. The nontrivial topology results in an anomalous charge transport. The charge transport is quantized and can be used to extract the Chern numbers experimentally. Our theory presents an entirely new mechanism for electric current generation induced by the motion of multiple-Q spin texture in magnetic insulators. Our results can be extended to 3D magnets with multiple- Q spin textures where even higher dimensional topological physics can be realized.

ACKNOWLEDGMENTS

We would like to thank Joel Moore, Chih-Chun Chien, and Cristian Batista for insightful discussions. Computer resources for numerical calculations were supported by the Institutional Computing Program at LANL. This work was carried out under the auspices of the U.S. DOE NNSA under contract No. 89233218CNA000001 through the LDRD Program, and was supported by the Center for Nonlinear Studies at LANL (Y. S. and S.Z.L). S.H. is supported by the JSPS KAKENHI Grants No. JP18K13488.

Appendix A: Semi-classical equation of motion

Here we consider a very general model of free electrons coupled to a periodic modulation potential described by

$$H_0 = \frac{\mathbf{p}^2}{2m} + \sum_{\mathbf{v}} V_{\mathbf{v}}(\mathbf{Q}_{\mathbf{v}} \cdot \mathbf{r}), \quad (\text{A1})$$

and we study how the electron dynamics is affected by the motion and deformation of the potential. The potential is the linear superposition of a set of periodic functions $V_{\mathbf{v}}(\mathbf{Q}_{\mathbf{v}} \cdot \mathbf{r})$ with the modulating vector $\mathbf{Q}_{\mathbf{v}}$. The perturbation can be induced by asking $V_{\mathbf{v}}(\mathbf{Q}_{\mathbf{v}} \cdot \mathbf{r}) \rightarrow V_{\mathbf{v}}(\mathbf{Q}_{\mathbf{v}} \cdot \mathbf{r} + \phi_{\mathbf{v}})$ where

$$\phi_{\mathbf{v}}(\mathbf{r}, \tau) = \omega_{\mathbf{v}}\tau + \mathbf{Q}'_{\mathbf{v}} \cdot \mathbf{r}. \quad (\text{A2})$$

Here the first term shifts the potential and the second term deforms the potential. Apparently, the multiple- Q spin texture model belongs to the category depicted by Eq. (A1). In the semi-classical approach, the electronic state is described by a wave packet that is highly localized at the center of mass \mathbf{r}_c and \mathbf{k}^c in the phase space. Due to the localized nature, when the perturbation is smooth compared to the length scale spread by the wave packet, the approximate Hamiltonian for the wave packet can be obtained by linearizing the perturbation as $\phi_{\mathbf{v}}(\mathbf{r}, \tau) \approx \phi_{\mathbf{v}}(\mathbf{r}_c, \tau)$ [35]. The leading order local Hamiltonian is

$$H_c = \frac{\mathbf{p}^2}{2m} + \sum_{\mathbf{v}} V_{\mathbf{v}}(\mathbf{Q}_{\mathbf{v}} \cdot \mathbf{r} + \phi_{\mathbf{v}}(\mathbf{r}_c, \tau)) \quad (\text{A3})$$

and the first order correction is $H_1 = \partial_{\mathbf{r}_c} H_c \cdot (\mathbf{r} - \mathbf{r}_c)$. Here we have

$$\dot{\phi}_{\mathbf{v}} = \omega_{\mathbf{v}} + \mathbf{Q}'_{\mathbf{v}} \cdot \dot{\mathbf{r}}_c, \quad (\text{A4})$$

that depends on the velocity of the wave packet. Because H_c has the same translation symmetry as H_0 , its eigenstates are still the Bloch states of H_0 as

$$|\psi_{n\mathbf{k}}(\tilde{\mathbf{r}})\rangle = e^{i\mathbf{k}_{\mu}\tilde{\mathbf{r}}^{\mu}} |u_{n\mathbf{k}}(\tilde{\mathbf{r}})\rangle \quad (\text{A5})$$

but with a shifted position $\tilde{\mathbf{r}}^{\mu} = r^{\mu} + \phi_{\mathbf{v}}/Q_{\nu\mu}$ due to $\phi_{\mathbf{v}}(\mathbf{r}_c, \tau)$.

The wave packet to the leading order can be constructed from the Bloch states as

$$|W_n\rangle = \int d\mathbf{k} w_n(\mathbf{k}, \tau) |\psi_{n\mathbf{k}}(\tilde{\mathbf{r}})\rangle, \quad (\text{A6})$$

where the electron dynamics is confined in a single band whose dispersion is $E_n(\mathbf{k})$ with n being the band index. The interband coupling is encoded in the higher order corrections and will be studied in the next section. In the following, we denote \mathbf{r}_n and \mathbf{k}^n as the center of mass of the wave packet $|W_n\rangle$ in the phase space. To be self-consistent, we have

$$k_{\mu}^n = \langle W_n | k_{\mu} | W_n \rangle = \int d\mathbf{k} |w_n(\mathbf{k}, \tau)|^2 k_{\mu} \quad (\text{A7})$$

that indicates $w_n(\mathbf{k}, \tau)$ is highly localized at \mathbf{k}^n , and

$$\begin{aligned} r_n^{\mu} &= \langle W_n | r^{\mu} | W_n \rangle = \int d\mathbf{k}' \int d\mathbf{k} w_n^*(\mathbf{k}', \tau) w_n(\mathbf{k}, \tau) \langle \psi_{n\mathbf{k}'}(\tilde{\mathbf{r}}) | (-i\partial_{k_{\mu}} e^{i\mathbf{k}_{\gamma}\tilde{\mathbf{r}}^{\gamma}}) e^{i\mathbf{k}_{\gamma}\phi_{\mathbf{v}}/Q_{\nu\gamma}} | u_{n\mathbf{k}}(\tilde{\mathbf{r}}) \rangle \\ &= -i \int d\mathbf{k}' \int d\mathbf{k} w_n^*(\mathbf{k}', \tau) w_n(\mathbf{k}, \tau) \langle \psi_{n\mathbf{k}'} | \partial_{k_{\mu}} | \psi_{n\mathbf{k}} \rangle - \phi_{\mathbf{v}}/Q_{\nu\mu} + i \int d\mathbf{k}' \int d\mathbf{k} w_n^*(\mathbf{k}', \tau) w_n(\mathbf{k}, \tau) \langle \psi_{n\mathbf{k}'} | e^{i\mathbf{k}_{\gamma}\tilde{\mathbf{r}}^{\gamma}} | \partial_{k_{\mu}} u_{n\mathbf{k}} \rangle \\ &= -\partial_{k_{\mu}^n} \arg[w(\mathbf{k}^n, \tau)] - \phi_{\mathbf{v}}/Q_{\nu\mu} + i \langle u_{n\mathbf{k}^n} | \partial_{k_{\mu}^n} u_{n\mathbf{k}^n} \rangle \end{aligned} \quad (\text{A8})$$

where we have used the integration by parts and the fact that

$$\begin{aligned} &\langle \psi_{n\mathbf{k}'}(\tilde{\mathbf{r}}) | e^{i\mathbf{k}_{\gamma}\tilde{\mathbf{r}}^{\gamma}} | \partial_{k_{\mu}} u_{n\mathbf{k}}(\tilde{\mathbf{r}}) \rangle \\ &= \frac{1}{N} \sum_{\mathbf{R}} e^{i(\mathbf{k}-\mathbf{k}')\cdot\mathbf{R}} \frac{1}{s_0} \int_{\text{UC}} d\xi u_{n\mathbf{k}'}(\xi) e^{i(\mathbf{k}-\mathbf{k}')\cdot\xi} \partial_{k_{\mu}} u_{n\mathbf{k}}(\xi) \quad (\text{A9}) \\ &= \delta(\mathbf{k}-\mathbf{k}') \langle u_{n\mathbf{k}'}(\xi) | e^{i(\mathbf{k}-\mathbf{k}')\cdot\xi} | \partial_{k_{\mu}} u_{n\mathbf{k}}(\xi) \rangle. \end{aligned}$$

Here N is the number of unit cells (UC), s_0 is the area of a UC, and we parameterize $\tilde{\mathbf{r}} = \mathbf{R} + \xi$ where \mathbf{R} is the lattice vector and ξ is within the UC centered at the origin. Therefore $\int d\tilde{\mathbf{r}} = \sum_{\mathbf{R}} \int_{\text{UC}} d\xi$ since $u_{n\mathbf{k}}(\mathbf{R} + \xi) = u_{n\mathbf{k}}(\xi)$.

The equation of motion can be obtained from the La-

grangian $L = \langle W_n | i\hbar\partial_\tau - H | W_n \rangle$. For the first term, we have

$$\begin{aligned} \langle W_n | i\hbar\partial_\tau | W_n \rangle &= \int d\mathbf{k}' \int d\mathbf{k} w_n^*(\mathbf{k}', \tau) \langle \psi_{n\mathbf{k}'}(\tilde{\mathbf{r}}) | i\hbar\partial_\tau w_n(\mathbf{k}, \tau) e^{i\mathbf{k}_\mu \tilde{\mathbf{r}}^\mu} | u_{n\mathbf{k}}(\tilde{\mathbf{r}}) \rangle \\ &= i\hbar \int d\mathbf{k} w_n^*(\mathbf{k}, \tau) \partial_\tau w_n(\mathbf{k}, \tau) - \hbar \int d\mathbf{k} |w_n(\mathbf{k}, \tau)|^2 k_\mu \dot{\phi}_\nu / Q_{\nu\mu} + i\hbar \int d\mathbf{k} |w_n(\mathbf{k}, \tau)|^2 \langle u_{n\mathbf{k}}(\tilde{\mathbf{r}}) | \partial_\tau u_{n\mathbf{k}}(\tilde{\mathbf{r}}) \rangle \\ &= -\hbar \partial_\tau \arg[w_n(\mathbf{k}^n, \tau)] - \hbar k_\mu^n \dot{\phi}_\nu / Q_{\nu\mu} + i\hbar \dot{\phi}_\nu \langle u_{n\mathbf{k}^n} | \partial_{\phi_\nu} u_{n\mathbf{k}^n} \rangle \\ &= \hbar k_\mu^n \partial_{k_\mu^n} \arg[w_n(\mathbf{k}^n, \tau)] - \hbar k_\mu^n \dot{\phi}_\nu / Q_{\nu\mu} + i\hbar \dot{\phi}_\nu \langle u_{n\mathbf{k}^n} | \partial_{\phi_\nu} u_{n\mathbf{k}^n} \rangle \end{aligned} \quad (\text{A10})$$

where we use the fact that $-\hbar \partial_\tau \arg[w_n(\mathbf{k}^n, \tau)] = -\hbar \frac{d}{dt} \arg[w_n(\mathbf{k}^n, \tau)] + \hbar k_\mu^n \partial_{k_\mu^n} \arg[w_n(\mathbf{k}^n, \tau)]$ and the total time derivative is dropped because it just contributes a constant to the action and does not affect the equation of motion. To the leading order, the second term of the Lagrangian is

$$\langle W_n | H | W_n \rangle \approx \langle W_n | H_c | W_n \rangle = E_n(\mathbf{k}^n). \quad (\text{A11})$$

Now we combine Eq. (A8) and Eq. (A10) together that yields the final expression of the Lagrangian

$$\begin{aligned} L(\mathbf{r}_n, \dot{\mathbf{r}}_n, \mathbf{k}^n, \dot{\mathbf{k}}^n) &= \hbar k_\mu^n \left(-r_n^\mu - \phi_\nu / Q_{\nu\mu} + i \langle u_{n\mathbf{k}^n} | \partial_{k_\mu^n} u_{n\mathbf{k}^n} \rangle \right) \\ &- \hbar k_\mu^n \dot{\phi}_\nu / Q_{\nu\mu} + i\hbar \dot{\phi}_\nu \langle u_{n\mathbf{k}^n} | \partial_{\phi_\nu} u_{n\mathbf{k}^n} \rangle - E_n(\mathbf{k}^n). \end{aligned} \quad (\text{A12})$$

According to the Euler-Lagrange equation, the leading order semi-classical equation of the motion is

$$\begin{aligned} \dot{r}_n^\mu &= \frac{\partial E_n(\mathbf{k}^n)}{\hbar \partial k_\mu^n} - k_\gamma^n \Omega_{n,kk}^{\mu\gamma} - \dot{\phi}_\nu \Omega_{n,k\phi}^{\mu\nu}, \\ \dot{k}_\mu^n &= 0. \end{aligned} \quad (\text{A13})$$

where the Berry curvatures

$$\Omega_{n,kk}^{\mu\gamma} = i \left(\partial_{k_\mu^n} \langle u_{n\mathbf{k}^n} | \partial_{k_\gamma^n} u_{n\mathbf{k}^n} \rangle - \partial_{k_\gamma^n} \langle u_{n\mathbf{k}^n} | \partial_{k_\mu^n} u_{n\mathbf{k}^n} \rangle \right), \quad (\text{A14})$$

$$\Omega_{n,k\phi}^{\mu\nu} = i \left(\partial_{k_\mu^n} \langle u_{n\mathbf{k}^n} | \partial_{\phi_\nu} u_{n\mathbf{k}^n} \rangle - \partial_{\phi_\nu} \langle u_{n\mathbf{k}^n} | \partial_{k_\mu^n} u_{n\mathbf{k}^n} \rangle \right), \quad (\text{A15})$$

are respectively defined in the crystal momentum space and the hybrid momentum space consist of the crystal momentum k_μ^n and phason mode ϕ_ν . In this sense, ϕ_ν does play the same role as the crystal momentum and the space dimension is transcendent accordingly. The dynamics of ϕ_ν follows Eq. (A4) which is part of the equation of motion. The new contribution $-\dot{\phi}_\nu \Omega_{n,k\phi}^{\mu\nu}$ to the velocity of wave packet is due to the translational motion of the periodically modulated potential.

Appendix B: Higher order corrections to the equation of motion

To include the higher order corrections to the equation of motion, we consider the wave packet with the first order corrections. According to the perturbation theory, the eigenstate of $H_c + H_1$ up to the first order is

$$\begin{aligned} |\psi_{n\mathbf{k}}(\tilde{\mathbf{r}})\rangle &= e^{i\mathbf{k}_\mu \tilde{\mathbf{r}}^\mu} \left(|u_{n\mathbf{k}}(\tilde{\mathbf{r}})\rangle + \sum_{m \neq n} c_m(\mathbf{k}) |u_{m\mathbf{k}}(\tilde{\mathbf{r}})\rangle \right) \\ &= e^{i\mathbf{k}_\mu \tilde{\mathbf{r}}^\mu} \left(|u_{n\mathbf{k}}(\tilde{\mathbf{r}})\rangle + |u_{n\mathbf{k}}^{(1)}(\tilde{\mathbf{r}})\rangle \right), \end{aligned} \quad (\text{B1})$$

where $|u_{n\mathbf{k}}^{(1)}(\tilde{\mathbf{r}})\rangle$ is the first order correction to the eigenstate and

$$c_m(\mathbf{k}) = \frac{\langle u_{m\mathbf{k}}(\tilde{\mathbf{r}}) | H_1 | u_{n\mathbf{k}}(\tilde{\mathbf{r}}) \rangle}{E_n(\mathbf{k}) - E_m(\mathbf{k})}. \quad (\text{B2})$$

Thus the wave packet should be constructed from the corrected eigenstates as

$$|W_n\rangle = |W_n^{(0)}\rangle + |W_n^{(1)}\rangle = \int d\mathbf{k} w_n(\mathbf{k}, \tau) e^{i\mathbf{k}_\mu \tilde{\mathbf{r}}^\mu} \left(|u_{n\mathbf{k}}(\tilde{\mathbf{r}})\rangle + |u_{n\mathbf{k}}^{(1)}(\tilde{\mathbf{r}})\rangle \right) \quad (\text{B3})$$

The self-consistent conditions of the wave packet are still $k_\mu^n = \langle W_n | k_\mu | W_n \rangle$ and

$$r_n^\mu = \langle W_n^{(0)} | r^\mu | W_n^{(0)} \rangle + \langle W_n^{(0)} | r^\mu | W_n^{(1)} \rangle + \langle W_n^{(1)} | r^\mu | W_n^{(0)} \rangle \quad (\text{B4})$$

up to the first order. Here the first term is the same as Eq. (A8) and the second term is

$$\langle W_n^{(0)} | r^\mu | W_n^{(1)} \rangle = i \langle u_{n\mathbf{k}^n} | \partial_{k_\mu^n} u_{n\mathbf{k}^n}^{(1)} \rangle, \quad (\text{B5})$$

where we use the fact that $\langle u_{n\mathbf{k}^n} | u_{n\mathbf{k}^n}^{(1)} \rangle = 0$. Therefore the center of mass is

$$\begin{aligned} r_n^\mu &= -\partial_{k_\mu^n} \arg[w_n(\mathbf{k}^n, \tau)] - \phi_\nu / Q_{\nu\mu} + i \langle u_{n\mathbf{k}^n} | \partial_{k_\mu^n} u_{n\mathbf{k}^n} \rangle \\ &+ i \langle u_{n\mathbf{k}^n} | \partial_{k_\mu^n} u_{n\mathbf{k}^n}^{(1)} \rangle + i \langle u_{n\mathbf{k}^n}^{(1)} | \partial_{k_\mu^n} u_{n\mathbf{k}^n} \rangle, \end{aligned} \quad (\text{B6})$$

and the first order corrections come from the interband coupling.

For the Lagrangian $L = \langle W_n | i\hbar\partial_\tau - H | W_n \rangle$, the first term now becomes

$$\begin{aligned} \langle W_n | i\hbar\partial_\tau | W_n \rangle &= \langle W_n^{(0)} | i\hbar\partial_\tau | W_n^{(0)} \rangle + \langle W_n^{(0)} | i\hbar\partial_\tau | W_n^{(1)} \rangle \\ &+ \langle W_n^{(1)} | i\hbar\partial_\tau | W_n^{(0)} \rangle \end{aligned} \quad (\text{B7})$$

where the leading order term $\langle W_n^{(0)} | i\hbar\partial_\tau | W_n^{(0)} \rangle$ is the same as Eq. (A10) and the first order correction is

$$\langle W_n^{(0)} | i\hbar\partial_\tau | W_n^{(1)} \rangle = i\hbar \dot{\phi}_\nu \langle u_{n\mathbf{k}^n} | \partial_{\phi_\nu} u_{n\mathbf{k}^n}^{(1)} \rangle. \quad (\text{B8})$$

The dispersion relation is corrected to the first order as

$$\langle W_n | H | W_n \rangle \approx \langle W_n | H_c + H_1 | W_n \rangle = \tilde{E}_n(\mathbf{k}^n). \quad (\text{B9})$$

Now the Lagrangian becomes

$$\begin{aligned}
L(\mathbf{r}_n, \dot{\mathbf{r}}_n, \mathbf{k}^n, \dot{\mathbf{k}}^n) &= \hbar \dot{k}_\mu^n \partial_{k_\mu^n} \arg[w_n(\mathbf{k}^n, \tau)] - \hbar k_\mu^n \dot{\phi}_\nu / Q_{\nu\mu} + i \hbar \dot{\phi}_\nu \langle u_{nk^n} | \partial_{\phi_\nu} u_{nk^n} \rangle + i \hbar \dot{\phi}_\nu \langle u_{nk^n} | \partial_{\phi_\nu} u_{nk^n}^{(1)} \rangle + i \hbar \dot{\phi}_\nu \langle u_{nk^n}^{(1)} | \partial_{\phi_\nu} u_{nk^n} \rangle \\
&= \hbar \dot{k}_\mu^n \left(-r_n^\mu - \phi_\nu / Q_{\nu\mu} + i \langle u_{nk^n} | \partial_{k_\mu^n} u_{nk^n} \rangle + i \langle u_{nk^n} | \partial_{k_\mu^n} u_{nk^n}^{(1)} \rangle + i \langle u_{nk^n}^{(1)} | \partial_{k_\mu^n} u_{nk^n} \rangle \right) - \hbar k_\mu^n \dot{\phi}_\nu / Q_{\nu\mu} \\
&\quad + i \hbar \dot{\phi}_\nu \langle u_{nk^n} | \partial_{\phi_\nu} u_{nk^n} \rangle + i \hbar \dot{\phi}_\nu \langle u_{nk^n} | \partial_{\phi_\nu} u_{nk^n}^{(1)} \rangle + i \hbar \dot{\phi}_\nu \langle u_{nk^n}^{(1)} | \partial_{\phi_\nu} u_{nk^n} \rangle
\end{aligned} \tag{B10}$$

according to Eq. (B6). The Euler-Lagrange equation yields the semi-classical equation of motion with the higher order corrections as

$$\begin{aligned}
\dot{r}_n^\mu &= \frac{\partial \tilde{E}_n(\mathbf{k}^n)}{\hbar \partial k_\mu^n} - \dot{k}_\nu^n \tilde{\Omega}_{n,kk}^{\mu\nu} - \dot{\phi}_\nu \tilde{\Omega}_{n,k\phi}^{\mu\nu}, \\
\dot{k}_\mu^n &= 0,
\end{aligned} \tag{B11}$$

where the Berry curvatures with the higher order corrections are

$$\begin{aligned}
\tilde{\Omega}_{n,kk}^{\mu\nu} &= \Omega_{n,kk}^{\mu\nu} + i \left(\partial_{k_\nu^n} \langle u_{nk^n} | \partial_{k_\mu^n} u_{nk^n}^{(1)} \rangle - \partial_{k_\mu^n} \langle u_{nk^n} | \partial_{k_\nu^n} u_{nk^n}^{(1)} \rangle \right) \\
&\quad + i \left(\partial_{k_\mu^n} \langle u_{nk^n}^{(1)} | \partial_{k_\nu^n} u_{nk^n} \rangle - \partial_{k_\nu^n} \langle u_{nk^n}^{(1)} | \partial_{k_\mu^n} u_{nk^n} \rangle \right),
\end{aligned} \tag{B12}$$

$$\begin{aligned}
\tilde{\Omega}_{n,k\phi}^{\mu\nu} &= \Omega_{n,k\phi}^{\mu\nu} + i \left(\partial_{k_\mu^n} \langle u_{nk^n} | \partial_{\phi_\nu} u_{nk^n}^{(1)} \rangle - \partial_{\phi_\nu} \langle u_{nk^n} | \partial_{k_\mu^n} u_{nk^n}^{(1)} \rangle \right) \\
&\quad + i \left(\partial_{k_\mu^n} \langle u_{nk^n}^{(1)} | \partial_{\phi_\nu} u_{nk^n} \rangle - \partial_{\phi_\nu} \langle u_{nk^n}^{(1)} | \partial_{k_\mu^n} u_{nk^n} \rangle \right).
\end{aligned} \tag{B13}$$

Apparently, the equation of motion with the higher order corrections are still in the same form as the leading order equation of motion derived in the section above. The modified dispersion relation and Berry curvature with first order corrections are induced by the interband coupling.

Appendix C: Unify the dummy index

In the notation above, the index $\nu = \{1, 2, \dots\}$ is for the ancillary dimensions associated with phason modes of the translational motion of the periodic modulation, while $\mu, \gamma = \{x, y\}$ are for the physical dimensions. To unify the dummy indices, we introduce the hybrid momentum space spanned by the generalized momentum

$$\tilde{\mathbf{k}} = (k_x, k_y, \phi_1, \phi_2, \dots). \tag{C1}$$

In the current notation, the equation of motion becomes

$$\dot{r}_n^\mu = \frac{\partial \tilde{E}_n(\tilde{\mathbf{k}})}{\hbar \partial \tilde{k}_\mu} - \dot{\tilde{k}}_\nu \tilde{\Omega}_n^{\mu\nu}, \tag{C2}$$

where the superscript of $\tilde{\mathbf{k}}^n$ is dropped hereafter and in the main text for simplification. Now $\mu, \nu, \gamma = \{x, y, 1, 2, \dots\}$ are equivalent. However, Eq. (C2) is meaningful only for $\mu = x$ or y since the center of mass \mathbf{r}_n is confined in the real space. Here the unified Berry curvature is

$$\begin{aligned}
\tilde{\Omega}_n^{\mu\nu} &= \Omega_n^{\mu\nu} + \Omega_n^{(1)\mu\nu}, \\
\Omega_n^{\mu\nu} &= i \left(\partial_{\tilde{k}_\mu} \langle u_{n\tilde{\mathbf{k}}} | \partial_{\tilde{k}_\nu} u_{n\tilde{\mathbf{k}}} \rangle - \partial_{\tilde{k}_\nu} \langle u_{n\tilde{\mathbf{k}}} | \partial_{\tilde{k}_\mu} u_{n\tilde{\mathbf{k}}} \rangle \right), \\
\Omega_n^{(1)\mu\nu} &= i \left(\partial_{\tilde{k}_\mu} \langle u_{n\tilde{\mathbf{k}}} | \partial_{\tilde{k}_\nu} u_{n\tilde{\mathbf{k}}}^{(1)} \rangle - \partial_{\tilde{k}_\nu} \langle u_{n\tilde{\mathbf{k}}} | \partial_{\tilde{k}_\mu} u_{n\tilde{\mathbf{k}}}^{(1)} \rangle \right) \\
&\quad + i \left(\partial_{\tilde{k}_\mu} \langle u_{n\tilde{\mathbf{k}}}^{(1)} | \partial_{\tilde{k}_\nu} u_{n\tilde{\mathbf{k}}} \rangle - \partial_{\tilde{k}_\nu} \langle u_{n\tilde{\mathbf{k}}}^{(1)} | \partial_{\tilde{k}_\mu} u_{n\tilde{\mathbf{k}}} \rangle \right),
\end{aligned} \tag{C3}$$

where $\Omega_n^{\mu\nu}$ is the leading order Berry curvature and $\Omega_n^{(1)\mu\nu}$ is the first order correction to the Berry curvature. The dynamics of the generalized momentum follows

$$\dot{\tilde{k}}_\nu = \begin{cases} 0, & \text{for } \nu = x, y \\ \omega_\nu + Q'_{\nu\gamma} \dot{r}_n^\gamma, & \text{for } \nu = 1, 2, \dots \end{cases} \tag{C4}$$

The deformation of the periodic modulation potential couples $\dot{\tilde{k}}_\nu$ with \dot{r}_n^γ that results in the nonlinear response of the system to the deformation. The nonlinear response function will be derived in the next section.

Appendix D: Nonlinear response function

The current density due to the motion and deformation of periodic modulation potential (induced by spin textures) is

$$j^\mu = e \sum_n \int d^2 k r_n^\mu f(E_n - E_F) D_n(\mathbf{r}, \tilde{\mathbf{k}}) \tag{D1}$$

where $D_n(\mathbf{r}, \tilde{\mathbf{k}})$ is the phase space density of states (PSDOS). In the absence of deformation, the phase space is homogeneous and the PSDOS is a constant as $D_n = 1/(2\pi)^d$ where d is the dimension of the system. However, due to the deformation, the phase space is inhomogeneous and we need to consider the modification of PSDOS. The basic idea is to study the time evolution of phase space volume element $\Delta V = \Delta \mathbf{r} \Delta \tilde{\mathbf{k}}$ that follows $(1/\Delta V) d\Delta V/dt = \nabla_{\mathbf{r}} \cdot \dot{\mathbf{r}} + \nabla_{\tilde{\mathbf{k}}} \cdot \dot{\tilde{\mathbf{k}}}$ [50]. The equation can be solved [51] and yields the modified PSDOS

$$\begin{aligned}
D_n(\mathbf{r}, \tilde{\mathbf{k}}) &= \frac{1}{\Delta V} = \frac{1}{(2\pi)^2} \left(1 + \frac{1}{2} Q'_{\mu\nu} \tilde{\Omega}_n^{\nu\mu} + \right. \\
&\quad \left. \frac{1}{64} \varepsilon^{\mu\nu\gamma\delta} Q'_{\mu\nu} Q'_{\gamma\delta} \varepsilon_{\eta\rho\alpha\beta} \tilde{\Omega}_n^{\eta\rho} \tilde{\Omega}_n^{\alpha\beta} \right),
\end{aligned} \tag{D2}$$

where $\varepsilon^{\mu\nu\gamma\delta}$ and $\varepsilon_{\eta\rho\alpha\beta}$ are Levi-Civita tensor with $\varepsilon^{xy12} = \varepsilon_{xy12} = 1$. Plugging Eq. (C4) into Eq. (C2) and retaining the terms up to the second order in ω_ν and $Q'_{\nu\mu}$ yields

$$\dot{r}_n^\mu = \frac{\partial \tilde{E}_n}{\hbar \partial k_\mu} - \omega_\nu \tilde{\Omega}_n^{\mu\nu} - \left(\frac{\partial \tilde{E}_n}{\hbar \partial k_\gamma} - \omega_\delta \tilde{\Omega}_n^{\gamma\delta} - \frac{\partial \tilde{E}_n}{\hbar \partial k_\eta} Q'_{\delta\eta} \tilde{\Omega}_n^{\gamma\delta} \right) Q'_{\nu\gamma} \tilde{\Omega}_n^{\mu\nu}, \tag{D3}$$

which is in the same form of Eq. (8) but with modified dispersion relation and Berry curvature due to the first order corrections. In the following, we will show that our finally results are not changed by the first order corrections which can be dropped. Now we substitute Eq. (D2) and Eq. (D3) into Eq. (D1) and retain the terms up the second order in ω_ν and $Q'_{\nu\mu}$ that gives

$$\begin{aligned}
j^\mu = e \sum_n \int \frac{d^2k}{(2\pi)^2} f(\tilde{E}_n - E_F) & \left[\left(\frac{\partial \tilde{E}_n}{\hbar \partial k_\mu} - \omega_\nu \tilde{\Omega}_n^{\mu\nu} \right) + \left(\omega_\delta \Omega_n^{\gamma\delta} Q'_{\nu\gamma} \Omega_n^{\mu\nu} - \frac{1}{2} \omega_\nu \Omega_n^{\mu\nu} Q'_{\gamma\delta} \Omega_n^{\delta\gamma} \right) - \left(\frac{\partial \tilde{E}_n}{\hbar \partial k_\gamma} Q'_{\nu\gamma} \tilde{\Omega}_n^{\mu\nu} - \frac{1}{2} \frac{\partial \tilde{E}_n}{\hbar \partial k_\mu} Q'_{\gamma\delta} \tilde{\Omega}_n^{\delta\gamma} \right) \right. \\
& \left. + \left(\frac{\partial E_n}{\hbar \partial k_\eta} Q'_{\delta\eta} \Omega_n^{\gamma\delta} Q'_{\nu\gamma} \Omega_n^{\mu\nu} - \frac{1}{2} \frac{\partial E_n}{\hbar \partial k_\gamma} Q'_{\nu\gamma} \Omega_n^{\mu\nu} Q'_{\eta\delta} \Omega_n^{\delta\eta} + \frac{1}{64} \frac{\partial E_n}{\hbar \partial k_\mu} \varepsilon^{\lambda\nu\gamma\delta} Q'_{\lambda\nu} Q'_{\gamma\delta} \varepsilon_{\eta\rho\alpha\beta} \Omega_n^{\eta\rho} \Omega_n^{\alpha\beta} \right) \right]. \quad (\text{D4})
\end{aligned}$$

Here we collect different terms with similar orders and forms into four groups enclosed by brackets. The integral of the first group just gives Eq. (4) where higher order corrections are dropped. Since we focus on the Fermi energy in the bulk energy gap that remains open upon weak perturbation, the modified group velocity $\partial_{k_\mu} \tilde{E}_n / \hbar$ and the first order correction to the Berry curvature $\Omega_n^{(1)\mu\nu}$ vanish under the integration over hybrid Brillouin zone [52]. Therefore, the transported charge described by Eq. (5) is unaffected by the higher order corrections. Notably, the second group in Eq. (D4) is unaffected by the higher order corrections. Because $\Omega_n^{\mu\nu} = -\Omega_n^{\nu\mu}$, $Q'_{\mu\nu} = -Q'_{\nu\mu}$, and the dummy indices can be freely replaced, we have

$$\begin{aligned}
& \omega_\delta \Omega_n^{\gamma\delta} Q'_{\nu\gamma} \Omega_n^{\mu\nu} - \frac{1}{2} \omega_\nu \Omega_n^{\mu\nu} Q'_{\gamma\delta} \Omega_n^{\delta\gamma} \\
& = \frac{\omega_\nu Q'_{\gamma\delta}}{2} \left(\Omega_n^{\mu\nu} \Omega_n^{\gamma\delta} + \Omega_n^{\mu\gamma} \Omega_n^{\delta\nu} + \Omega_n^{\mu\delta} \Omega_n^{\nu\gamma} \right) \quad (\text{D5})
\end{aligned}$$

for the second group. Here we use the transformation $\omega_\delta \Omega_n^{\gamma\delta} Q'_{\nu\gamma} \Omega_n^{\mu\nu} \rightarrow \omega_\nu \Omega_n^{\nu\gamma} Q'_{\gamma\delta} \Omega_n^{\mu\delta}$ under $\delta \leftrightarrow \nu$ and $\omega_\delta \Omega_n^{\gamma\delta} Q'_{\nu\gamma} \Omega_n^{\mu\nu} \rightarrow \omega_\nu \Omega_n^{\delta\nu} Q'_{\gamma\delta} \Omega_n^{\mu\gamma}$ under $\gamma \leftrightarrow \nu$ and then $\nu \leftrightarrow \delta$. Therefore, the integral of the first two groups yields the nonlinear response function Eq. (9).

Next, we are going to prove the integral of the last two groups are zero. For the third group, we use the same trick as above and we get

$$\begin{aligned}
& \frac{\partial \tilde{E}_n}{\hbar \partial k_\gamma} Q'_{\nu\gamma} \tilde{\Omega}_n^{\mu\nu} - \frac{1}{2} \frac{\partial \tilde{E}_n}{\hbar \partial k_\mu} Q'_{\gamma\delta} \tilde{\Omega}_n^{\delta\gamma} \\
& = \frac{Q'_{\gamma\delta}}{2\hbar} \left(\frac{\partial \tilde{E}_n}{\partial k_\mu} \tilde{\Omega}_n^{\gamma\delta} + \frac{\partial \tilde{E}_n}{\partial k_\gamma} \tilde{\Omega}_n^{\delta\mu} + \frac{\partial \tilde{E}_n}{\partial k_\delta} \tilde{\Omega}_n^{\mu\gamma} \right). \quad (\text{D6})
\end{aligned}$$

For a fully occupied band at zero temperature, the integral of Eq. (D6) yields

$$\frac{Q'_{\gamma\delta}}{2\hbar} \int d^2k \tilde{E}_n \left(\frac{\partial \tilde{\Omega}_n^{\gamma\delta}}{\partial k_\mu} + \frac{\partial \tilde{\Omega}_n^{\delta\mu}}{\partial k_\gamma} + \frac{\partial \tilde{\Omega}_n^{\mu\gamma}}{\partial k_\delta} \right), \quad (\text{D7})$$

where we use the integration by parts and the fact that both \tilde{E}_n and $\tilde{\Omega}_n^{\mu\nu}$ are periodic over the Brillouin zone. The three terms in the bracket equal to zero according to the Bianchi identity [53]. Therefore, the third group in Eq. (D4) does not contribute to the current density. The last group vanishes due to the antisymmetric property of $\Omega_n^{\mu\nu}$ and $Q'_{\mu\nu}$. To show the three terms are indeed canceled out, we take j^y as an example and we collect all the terms associated with $\frac{\partial \tilde{E}_n}{\hbar \partial k_y} Q'_{1y} Q'_{2x}$. Here the first two terms give

$$\frac{\partial E_n}{\hbar \partial k_y} Q'_{1y} Q'_{2x} \left(\Omega_n^{x1} \Omega_n^{y2} - \Omega_n^{y1} \Omega_n^{x2} \right) \quad (\text{D8})$$

and the last term yields

$$\frac{\partial E_n}{\hbar \partial k_y} Q'_{1y} Q'_{2x} \left(-\Omega_n^{x1} \Omega_n^{y2} + \Omega_n^{y1} \Omega_n^{x2} \right) \quad (\text{D9})$$

where we use the property $\Omega_n^{\mu\nu} Q'_{\gamma\delta} = \Omega_n^{\nu\mu} Q'_{\delta\gamma}$, $\Omega_n^{\mu\nu} \Omega_n^{\gamma\delta} = \Omega_n^{\nu\mu} \Omega_n^{\delta\gamma}$, and $Q'_{\mu\nu} Q'_{\gamma\delta} = Q'_{\nu\mu} Q'_{\delta\gamma}$. Obviously, Eq. (D8) and Eq. (D9) are opposite to each other, and the last group has no contribution to the current density.

Appendix E: Monte Carlo simulation

We present details of the model and numerical simulations for the spin textures. We here consider two models in order to describe three multiple- Q states: one is the effective spin model derived from the Kondo lattice model for the double- Q and triple- Q collinear spin textures and the other is the frustrated spin model for the triple- Q skyrmion spin texture.

The effective spin model is given by [54, 55]

$$\begin{aligned}
\mathcal{H} = 2 \sum_{\nu} & \left[-\tilde{J} \left\{ \alpha (S_{\mathcal{Q}_\nu}^x S_{-\mathcal{Q}_\nu}^x + S_{\mathcal{Q}_\nu}^y S_{-\mathcal{Q}_\nu}^y) + S_{\mathcal{Q}_\nu}^z S_{-\mathcal{Q}_\nu}^z \right\} \right. \\
& \left. + \tilde{K} \left\{ \alpha (S_{\mathcal{Q}_\nu}^x S_{-\mathcal{Q}_\nu}^x + S_{\mathcal{Q}_\nu}^y S_{-\mathcal{Q}_\nu}^y) + S_{\mathcal{Q}_\nu}^z S_{-\mathcal{Q}_\nu}^z \right\}^2 \right] - A \sum_i (S_i^z)^2, \quad (\text{E1})
\end{aligned}$$

where \mathbf{S}_q is the Fourier transform of \mathbf{S}_i and \mathcal{Q}_ν [$\nu = 1, 2$ (1, 2, 3) for the square (triangular) lattice] are the equivalent wave vectors for the multiple peaks in the bare susceptibility of itinerant electrons. The bilinear interaction $\tilde{J} = 1$ represents the effective Ruderman-Kittel-Kasuya-Yosida interaction and the positive biquadratic interaction $K = N\tilde{K}$ with N the number of sites represents the four-spin interactions leading to the multiple- Q instability. α is introduced as the anisotropy parameter for exchange coupling where $\alpha = 0$ represents the Ising-type coupling. The third term represents the easy-axis anisotropy ($A > 0$) for localized spins.

The simulations for the effective spin model are carried out with the classical Monte Carlo simulations at low temperatures. Our simulations are carried out with the standard Metropolis local updates. The results are obtained for systems with $N = 96 \times 96$ sites under periodic boundary conditions. In each simulation, we perform simulated annealing to find the low-energy spin configuration by gradually reducing the temperature with the rate $T_{n+1} = aT_n$, where T_n is the temperature in the n th step. We set the initial temperature $T_0 = 1.0 - 10.0$. We take $a = 0.99995-0.99999$ and the final temperature is typically taken at $T = 0.001-0.01$. We also start the simulations from the multiple- Q spin configurations, such as the double- Q and triple- Q collinear spin textures. We

determine the magnetic phase by comparing their energies of the obtained magnetic patterns in simulations. The double- Q collinear spin texture in Fig. 1(a) is obtained at $T = 0.01$, $K = 0.5$, $\alpha = 1.0$, $A = 0.5$, and $|\mathbf{Q}| = 2\pi/6$ on the square lattice, while the triple- Q collinear spin texture in Fig. 1(b) is obtained at $T = 0.001$, $K = 1.0$, $\alpha = 0.0$, $A = 0.0$, and $|\mathbf{Q}| = 2\pi/6$ on the triangular lattice.

The frustrated spin model on the triangular lattice is given by [56]

$$\mathcal{H} = \sum_{\langle i,j \rangle} J_{ij} \mathbf{S}_i \cdot \mathbf{S}_j - H \sum_i S_i^z - A \sum_i (S_i^z)^2, \quad (\text{E2})$$

where we consider the ferromagnetic nearest-neighbor coupling $J_1 = -1$ and antiferromagnetic third nearest-neighbor coupling $J_3 = 0.5$ in the first term, which gives the ordering vector $|\mathbf{Q}| = 2\pi/5$. The second and third terms represent the Zeeman coupling to an external magnetic field and the easy-axis anisotropy, respectively.

The optimal magnetic phases in the frustrated spin model are obtained from the Monte Carlo simulations based on the Metropolis algorithm. The lattices have $N = 100 \times 100$ spins and the periodic boundary conditions. In the simulations, the $10^5 - 10^7$ Monte Carlo sweeps measurements are performed after equilibration. The triple- Q skyrmion spin texture in Fig. 1(c) is obtained at $T = 0.01$, $H = 0.27$, and $A = 0.5$.

Appendix F: Time-dependent current

In the lattice model, the current through a bond connecting lattice sites i and j is

$$I_{ij}(\tau) = -i \frac{e}{\hbar} \sum_{E_n \leq E_F, \sigma} \langle \psi_n(\tau) | c_{i,\sigma}^\dagger t_{ij} c_{j,\sigma} - c_{j,\sigma}^\dagger t_{ji} c_{i,\sigma} | \psi_n(\tau) \rangle, \quad (\text{F1})$$

where $\sigma = \uparrow$ or \downarrow for spin degree of freedom and $|\psi_n(\tau)\rangle$ is the time evolution of the eigenstate $|\psi_n\rangle$ that is obtained by exact diagonalization of the Hamiltonian Eq. (1) at $\tau = 0$. The time evolution of eigenstates follows the time-dependent Schrödinger equation $i\hbar \partial_\tau |\psi_n(\tau)\rangle = \mathcal{H}(\tau) |\psi_n(\tau)\rangle$, which is solved numerically by the Runge-Kutta method. The total current I_x (I_y) is the sum of all the bond currents through a cross section perpendicular to the x (y) direction.

Appendix G: Anomalous charge transport for the spin texture ansatz

To compare with the numerical results for the spin textures from Monte Carlo simulation, we study the anomalous charge transport for the spin texture ansatz described by

$$\mathbf{S}_i = \left(0, 0, \sum_{\nu} \cos(\mathbf{Q}_\nu \cdot \mathbf{r}_i + \phi_\nu) \right). \quad (\text{G1})$$

The spin texture ansatz is exactly periodic and hence well quantized anomalous charge transport is expected.

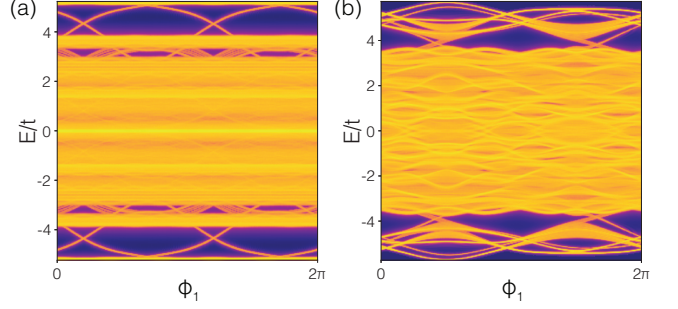


FIG. 4. Electronic spectral functions of the magnets with the double- Q collinear spin texture (a) and triple- Q collinear spin texture (b) depicted by the ansatz as a function of ϕ_1 . Here the purple (yellow) denotes low (high) density of states.

Here we consider a double- Q collinear spin texture with $\mathbf{Q}_1 = (2\pi/a, 0)$ and $\mathbf{Q}_2 = (0, 2\pi/a)$, and a triple- Q collinear spin texture with $\mathbf{Q}_1 = (-2\pi/a, 2\sqrt{3}\pi/a)$, $\mathbf{Q}_2 = (-2\pi/a, -2\sqrt{3}\pi/a)$, and $\mathbf{Q}_3 = (4\pi/a, 0)$. We first study the electronic spectrum to identify the topological property of the system. For conduction electrons hopping on a square lattice (whose lattice constant is set to unity), we fix $a = 5$ for both the double- Q and triple- Q spin textures depicted by Eq. (G1). While for the triple- Q spin texture, to make it commensurate with the lattice, we compress the lattice constant along the y direction to $1/\sqrt{3}$ such that each supercell also contains 5×5 lattice sites. The energy spectra as a function of ϕ_1 for the double- Q and triple- Q spin textures when $J = 1.5t$ and $B = 0$ in Eq. (1) are shown in Figs. 4(a) and 4(b), respectively. Here we use the open boundary condition along the x direction and the periodic boundary condition along the y direction. Apparently, there are topological edge states in the bulk energy gaps indicating the system is topologically nontrivial. To characterize the nontrivial topology, we calculate the Chern numbers of the system. Here we focus on the Fermi energy in the bottom bulk energy gaps in Fig. 4. In the 4D hybrid momentum space of the double- Q spin texture, there are six first Chern numbers: $C_1^{x1} = C_1^{y2} = 2$ and $C_1^{xy} = C_1^{x2} = C_1^{y1} = C_1^{12} = 0$, and one second Chern number: $C_2^{x1y2} = -2$. In the 5D hybrid momentum space of the triple- Q spin texture, there are ten first Chern numbers: $C_1^{x1} = C_1^{x2} = -C_1^{y1} = C_1^{y2} = -2$ and $C_1^{xy} = C_1^{x3} = C_1^{y3} = C_1^{12} = C_1^{13} = C_1^{23} = 0$, and five second Chern numbers: $C_2^{x1y2} = -2$ and $C_2^{xy13} = C_2^{xy23} = C_2^{x123} = C_2^{y123} = 0$. The first Chern numbers on different 2D planes and second Chern numbers on different 4D hypersurfaces are independent of the other momenta because the bulk energy gaps are open in the entire hybrid momentum space.

We then study the anomalous charge transport induced by the translational motion of the spin textures, which is parameterized by $\phi_\nu = \omega_\nu \tau$. Here we consider the spin texture moving in the y direction same as that in the main text. For the double- Q spin texture, we have $\omega_1 = 0$ and $\omega_2 = 2\pi t/100\hbar$, while for the triple- Q spin texture, we have $\omega_1 = -\omega_2 = 2\pi t/100\hbar$ and $\omega_3 = 0$. Thus the period of

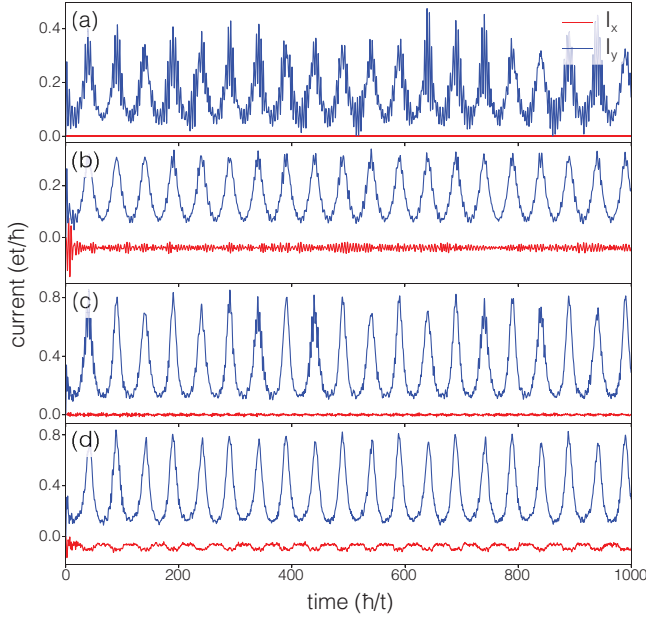


FIG. 5. Currents along the x and y directions for the magnets with multiple- Q collinear spin textures depicted by the ansatz. (a) and (b) Currents for the double- Q spin texture without and with deformation, respectively. (c) and (d) Currents for the triple- Q spin texture without and with deformation, respectively.

motion of both the double- Q and triple- Q spin textures is $\Delta\tau = 100\hbar/t$. We calculate the currents due to the motion of spin textures on a 40×40 lattice (containing 8×8 supercells). For the double- Q spin texture, the currents over

ten periods are shown in 5(a). By integrating the currents over time, the average transported charges in one period are quantized as $q^x = 0.00e$ and $q^y = 15.99e$. According to Eq. (5), the transported charges are $q^x = eN^x\omega_2C_1^{x2}/|\omega_2| = 0e$ and $q^y = eN^y\omega_2C_1^{y2}/|\omega_2| = 16e$. For the triple- Q spin texture, the currents over ten periods are shown in Fig. 5(c) that gives $q^x = 0.00e$ and $q^y = 31.97e$. The transported charges are $q^x = eN^x\omega_1C_1^{x1}/|\omega_1| + eN^x\omega_2C_1^{x2}/|\omega_2| = 0e$ and $q^y = eN^y\omega_1C_1^{y1}/|\omega_1| + eN^y\omega_2C_1^{y2}/|\omega_2| = 32e$ according to Eq. (5). Apparently, the numerical results show a very good agreement with Eq. (5).

To trigger the nonlinear response, one needs to deform the spin texture. For the double- Q spin texture, we apply a shear deformation of the spin texture by deforming the \mathbf{Q}_1 vector to $\mathbf{Q}_1 = (2\pi/5, 2\pi/20)$. By shifting the spin texture in the same way mentioned above, we obtain $q^x = -4.00e$ and $q^y = 16.00e$ from the currents in Fig. 5(b). The numerical results are also consistent with $q^x = eL^xC_2^{x21y}\omega_2Q'_{1y}/2\pi|\omega_2| = -4e$ and $q^y = 16e$ according to Eq. (10). For the triple- Q spin texture, we apply a shear deformation of the spin texture by deforming the \mathbf{Q}_v vectors to $\mathbf{Q}_1 = (-2\pi/5, 2\sqrt{3}\pi/5 - 2\sqrt{3}\pi/20)$, $\mathbf{Q}_2 = (-2\pi/5, -2\sqrt{3}\pi/5 - 2\sqrt{3}\pi/20)$, and $\mathbf{Q}_3 = (4\pi/5, 2\sqrt{3}\pi/10)$. In this case, the currents over ten periods are shown in Fig. 5(d) that gives $q^x = -7.98e$ and $q^y = 31.96e$. Eq. (5) yields $q^x = eL^xC_2^{x21y}\omega_1Q'_{2y}/2\pi|\omega_1| + eL^xC_2^{x21y}\omega_2Q'_{1y}/2\pi|\omega_2| = -8e$ and $q^y = 32e$ as before that agree with the numerical results. The numerical results of anomalous charge transport for the spin texture ansatz are perfectly quantized and exhibit very good agreement with the response function.

-
- [1] S. Mühlbauer, B. Binz, F. Jonietz, C. Pfleiderer, A. Rosch, A. Neubauer, R. Georgii, and P. Böni, “Skyrmion lattice in a chiral magnet,” *Science* **323**, 915 (2009).
- [2] X. Z. Yu, Y. Onose, N. Kanazawa, J. H. Park, J. H. Han, Y. Matsui, N. Nagaosa, and Y. Tokura, “Real-space observation of a two-dimensional skyrmion crystal,” *Nature* **465**, 901 (2010).
- [3] Stefan Heinze, Kirsten von Bergmann, Matthias Menzel, Jens Brede, Roland Kubetzka, Andréand Wiesendanger, Gustav Bihlmayer, and Stefan Blügel, “Spontaneous atomic-scale magnetic skyrmion lattice in two dimensions,” *Nature Physics* **7**, 713 (2011).
- [4] S. Seki, X. Z. Yu, S. Ishiwata, and Y. Tokura, “Observation of skyrmions in a multiferroic material,” *Science* **336**, 198 (2012).
- [5] F. Jonietz, S. Mühlbauer, C. Pfleiderer, A. Neubauer, W. Münzer, A. Bauer, T. Adams, R. Georgii, P. Böni, R. A. Duine, K. Everschor, M. Garst, and A. Rosch, “Spin transfer torques in MnSi at ultralow current densities,” *Science* **330**, 1648 (2010).
- [6] X. Z. Yu, N. Kanazawa, W. Z. Zhang, T. Nagai, T. Hara, K. Kimoto, Y. Matsui, Y. Onose, and Y. Tokura, “Skyrmion flow near room temperature in an ultralow current density,” *Nat. Commun.* **3**, 988 (2012).
- [7] T. Schulz, R. Ritz, A. Bauer, M. Halder, M. Wagner, C. Franz, C. Pfleiderer, K. Everschor, M. Garst, and A. Rosch, “Emergent electrodynamics of skyrmions in a chiral magnet,” *Nat. Phys.* **8**, 301 (2012).
- [8] J. S. White, I. Levatic, A. A. Omrani, N. Egetenmeyer, K. Prsa, I. Zivkovic, J. L. Gavilano, J. Kohlbrecher, M. Bartkowiak, H. Berger, and H. M. Ronnow, “Electric field control of the skyrmion lattice in Cu_2OSeO_3 ,” *J. Phys.: Condens. Matter* **24**, 432201 (2012).
- [9] Ye-Hua Liu, You-Quan Li, and Jung Hoon Han, “Skyrmion dynamics in multiferroic insulators,” *Phys. Rev. B* **87**, 100402 (2013).
- [10] Weiwei Wang, Marijan Beg, Bin Zhang, Wolfgang Kuch, and Hans Fangohr, “Driving magnetic skyrmions with microwave fields,” *Phys. Rev. B* **92**, 020403 (2015).
- [11] SL Zhang, WW Wang, DM Burn, H Peng, H Berger, A Bauer, C Pfleiderer, G van der Laan, and T Hesjedal, “Manipulation of skyrmion motion by magnetic field gradients,” *Nature communications* **9**, 2115 (2018).
- [12] Lingyao Kong and Jiadong Zang, “Dynamics of an insulating skyrmion under a temperature gradient,” *Phys. Rev. Lett.* **111**, 067203 (2013).
- [13] Shi-Zeng Lin, Cristian D. Batista, Charles Reichhardt, and Avadh Saxena, “ac current generation in chiral magnetic insulators and skyrmion motion induced by the spin Seebeck effect,” *Phys. Rev. Lett.* **112**, 187203 (2014).

- [14] Y Onose, T Ideue, H Katsura, Y Shiomi, N Nagaosa, and Y Tokura, "Observation of the magnon hall effect," *Science* **329**, 297–299 (2010).
- [15] A. Chacon, A. Bauer, T. Adams, F. Rucker, G. Brandl, R. Georgii, M. Garst, and C. Pfleiderer, "Uniaxial pressure dependence of magnetic order in mnsi," *Phys. Rev. Lett.* **115**, 267202 (2015).
- [16] Y. Nii, T. Nakajima, A. Kikkawa, Y. Yamasaki, K. Ohishi, J. Suzuki, Y. Taguchi, T. Arima, Y. Tokura, and Y. Iwasa, "Uniaxial stress control of skyrmion phase," *Nature Communications* **6**, 8539 (2015).
- [17] K. Shibata, J. Iwasaki, N. Kanazawa, S. Aizawa, T. Tanigaki, M. Shirai, T. Nakajima, M. Kubota, M. Kawasaki, H. S. Park, D. Shindo, N. Nagaosa, and Y. Tokura, "Large anisotropic deformation of skyrmions in strained crystal," *Nature Nanotechnology* **10**, 589–592 (2015).
- [18] Albert Fert, Vincent Cros, and J. Sampaio, "Skyrmions on the track," *Nat. Nanotechnol.* **8**, 152–156 (2013).
- [19] Naoto Nagaosa and Yoshinori Tokura, "Topological properties and dynamics of magnetic skyrmions," *Nature Nanotechnology* **8**, 899–911 (2013).
- [20] Roland Wiesendanger, "Nanoscale magnetic skyrmions in metallic films and multilayers: a new twist for spintronics," *Nature Reviews Materials* **1**, 16044 (2016).
- [21] Naoto Nagaosa, Jairo Sinova, Shigeki Onoda, A. H. MacDonald, and N. P. Ong, "Anomalous hall effect," *Rev. Mod. Phys.* **82**, 1539–1592 (2010).
- [22] Ying Su and Shi-Zeng Lin, "Nontrivial topology and localization in the double exchange model with possible applications to perovskite manganites," *Phys. Rev. B* **98**, 235116 (2018).
- [23] A. Neubauer, C. Pfleiderer, B. Binz, A. Rosch, R. Ritz, P. G. Niklowitz, and P. Böni, "Topological hall effect in the a phase of MnSi," *Phys. Rev. Lett.* **102**, 186602 (2009).
- [24] Yufan Li, N. Kanazawa, X. Z. Yu, A. Tsukazaki, M. Kawasaki, M. Ichikawa, X. F. Jin, F. Kagawa, and Y. Tokura, "Robust formation of skyrmions and topological hall effect anomaly in epitaxial thin films of mnsi," *Phys. Rev. Lett.* **110**, 117202 (2013).
- [25] C. Franz, F. Freimuth, A. Bauer, R. Ritz, C. Schnarr, C. Duvinage, T. Adams, S. Blügel, A. Rosch, Y. Mokrousov, and C. Pfleiderer, "Real-space and reciprocal-space berry phases in the hall effect of $\text{mn}_{1-x}\text{fe}_x\text{si}$," *Phys. Rev. Lett.* **112**, 186601 (2014).
- [26] Ivar Martin and C. D. Batista, "Itinerant electron-driven chiral magnetic ordering and spontaneous quantum hall effect in triangular lattice models," *Phys. Rev. Lett.* **101**, 156402 (2008).
- [27] Cristian D. Batista, Shi-Zeng Lin, Satoru Hayami, and Yoshitomo Kamiya, "Frustration and chiral orderings in correlated electron systems," *Reports on Progress in Physics* **79**, 084504 (2016).
- [28] Sopheak Sorn, Stefan Divic, and Arun Paramakanti, "Tunable skyrmion crystals and topological quantum oscillations in magnetic metals," [arXiv:1810.08207 \[cond-mat\]](https://arxiv.org/abs/1810.08207) (2018), arXiv: 1810.08207.
- [29] Jiadong Zang, Maxim Mostovoy, Jung Hoon Han, and Naoto Nagaosa, "Dynamics of skyrmion crystals in metallic thin films," *Phys. Rev. Lett.* **107**, 136804 (2011).
- [30] Shi-Zeng Lin, Charles Reichhardt, Cristian D. Batista, and Avadh Saxena, "Driven skyrmions and dynamical transitions in chiral magnets," *Phys. Rev. Lett.* **110**, 207202 (2013).
- [31] Junichi Iwasaki, Masahito Mochizuki, and Naoto Nagaosa, "Current-induced skyrmion dynamics in constricted geometries," *Nature nanotechnology* **8**, 742 (2013).
- [32] S. E. Barnes and S. Maekawa, "Generalization of faraday's law to include nonconservative spin forces," *Phys. Rev. Lett.* **98**, 246601 (2007).
- [33] Shengyuan A. Yang, Geoffrey S. D. Beach, Carl Knutson, Di Xiao, Qian Niu, Maxim Tsoi, and James L. Erskine, "Universal electromotive force induced by domain wall motion," *Phys. Rev. Lett.* **102**, 067201 (2009).
- [34] Kjetil M. D. Hals and Arne Brataas, "Spin-motive forces and current-induced torques in ferromagnets," *Phys. Rev. B* **91**, 214401 (2015).
- [35] Di Xiao, Ming-Che Chang, and Qian Niu, "Berry phase effects on electronic properties," *Rev. Mod. Phys.* **82**, 1959–2007 (2010).
- [36] Chen Ning Yang, "Generalization of diracs monopole to su2 gauge fields," *Journal of Mathematical Physics* **19**, 320 (1978).
- [37] Takahiro Fukui, Yasuhiro Hatsugai, and Hiroshi Suzuki, "Chern numbers in discretized brillouin zone: efficient method of computing (spin) hall conductances," *Journal of the Physical Society of Japan* **74**, 1674–1677 (2005).
- [38] M Mochol-Grzelak, A Dauphin, A Celi, and M Lewenstein, "Efficient algorithm to compute the second chern number in four dimensional systems," *Quantum Science and Technology* **4**, 014009 (2018).
- [39] D. N. Sheng, L. Sheng, Z. Y. Weng, and F. D. M. Haldane, "Spin hall effect and spin transfer in a disordered rashba model," *Phys. Rev. B* **72**, 153307 (2005).
- [40] J. S. White, K. Prša, P. Huang, A. A. Omrani, I. Živković, M. Bartkowiak, H. Berger, A. Magrez, J. L. Gavilano, G. Nagy, J. Zang, and H. M. Rønnow, "Electric-field-induced skyrmion distortion and giant lattice rotation in the magnetoelectric insulator cu_2oseo_3 ," *Phys. Rev. Lett.* **113**, 107203 (2014).
- [41] D Okuyama, M Bleuel, JS White, Q Ye, J Krzywon, G Nagy, ZQ Im, I Živković, M Bartkowiak, HM Rønnow, et al., "Deformation of the moving magnetic skyrmion lattice in mnsi under electric current flow," *Communications Physics* **2**, 79 (2019).
- [42] A Garnier, D Gignoux, B Ouladdiaf, D Schmitt, and T Shigeoka, "Magnetic incommensurability in tetragonal DyRu_2Ge_2 ," *Physica B: Condensed Matter* **254**, 166–171 (1998).
- [43] Guy G. Marcus, Dae-Jeong Kim, Jacob A. Tutmaher, Jose A. Rodriguez-Rivera, Jonas Okkels Birk, Christof Niedermeyer, Hannah Lee, Zachary Fisk, and Collin L. Broholm, "Multi- q mesoscale magnetism in ceausb_2 ," *Phys. Rev. Lett.* **120**, 097201 (2018).
- [44] Wanjun Jiang, Pramey Upadhyaya, Wei Zhang, Guoqiang Yu, M. Benjamin Jungfleisch, Frank Y. Fradin, John E. Pearson, Yaroslav Tserkovnyak, Kang L. Wang, Olle Heinonen, Suzanne G. E. te Velthuis, and Axel Hoffmann, "Blowing magnetic skyrmion bubbles," *Science* **349**, 283–286 (2015).
- [45] Wanjun Jiang, Xichao Zhang, Guoqiang Yu, Wei Zhang, Xiao Wang, M. Benjamin Jungfleisch, John E. Pearson, Xuemei Cheng, Olle Heinonen, Kang L. Wang, Yan Zhou, Axel Hoffmann, and Suzanne G. E. te Velthuis, "Direct observation of the skyrmion Hall effect," *Nature Physics* **13**, 162–169 (2017).
- [46] Kai Litzius, Ivan Lemesh, Benjamin Krger, Pedram Bassirian, Lucas Caretta, Kornel Richter, Felix Bttner, Koji Sato, Oleg A. Tretiakov, Johannes Frster, Robert M. Reeve, Markus Weigand, Iuliia Bykova, Hermann Stoll, Gisela Schtz, Geoffrey S. D. Beach, and Mathias Klui, "Skyrmion Hall effect revealed by direct time-resolved X-ray microscopy," *Nature Physics* **13**, 170–175 (2017).
- [47] Qiming Shao, Yawen Liu, Guoqiang Yu, Se Kwon Kim, Xiaoyu Che, Chi Tang, Qing Lin He, Yaroslav Tserkovnyak, Jing Shi, and Kang L Wang, "Topological hall effect at above room temperature in heterostructures composed of a magnetic insulator and a heavy metal," *Nature Electronics* **2**, 182 (2019).

- [48] Shilei Ding, Andrew Ross, Romain Lebrun, Sven Becker, Kyujoon Lee, Isabella Boventer, Souvik Das, Yuichiro Kurokawa, Shruti Gupta, Jinbo Yang, et al., “Interfacial dzyaloshinskii-moriya interaction and chiral magnetic textures in a ferrimagnetic insulator,” [arXiv preprint arXiv:1906.07142](#) (2019).
- [49] Xiaopeng Li, W. Vincent Liu, and Leon Balents, “Spirals and skyrmions in two dimensional oxide heterostructures,” *Phys. Rev. Lett.* **112**, 067202 (2014).
- [50] Di Xiao, Junren Shi, and Qian Niu, “Berry phase correction to electron density of states in solids,” *Phys. Rev. Lett.* **95**, 137204 (2005).
- [51] H. M. Price, O. Zilberberg, T. Ozawa, I. Carusotto, and N. Goldman, “Four-dimensional quantum hall effect with ultracold atoms,” *Phys. Rev. Lett.* **115**, 195303 (2015).
- [52] Yang Gao, Shengyuan A. Yang, and Qian Niu, “Field induced positional shift of bloch electrons and its dynamical implications,” *Phys. Rev. Lett.* **112**, 166601 (2014).
- [53] Steven Weinberg, *Gravitation and Cosmology: Principles and Applications of* (John Wiley Sons, New York, 1972).
- [54] Satoru Hayami, Ryo Ozawa, and Yukitoshi Motome, “Effective bilinear-biquadratic model for noncoplanar ordering in itinerant magnets,” *Phys. Rev. B* **95**, 224424 (2017).
- [55] R. Takagi, J. S. White, S. Hayami, R. Arita, D. Honecker, H. M. Rønnow, Y. Tokura, and S. Seki, “Multiple-q non-collinear magnetism in an itinerant hexagonal magnet,” *Sci. Adv.* **4** (2018), 10.1126/sciadv.aau3402.
- [56] Satoru Hayami, Shi-Zeng Lin, and Cristian D. Batista, “Bubble and skyrmion crystals in frustrated magnets with easy-axis anisotropy,” *Phys. Rev. B* **93**, 184413 (2016).